Journal of Alloys and Compounds 837 (2020) 155496

Contents lists available at ScienceDirect

Journal of Alloys and Compounds

journal homepage: http://www.elsevier.com/locate/jalcom

# Structural investigation of the stability in temperature of some high entropy / multi major components alloys as a function of their electronic structure

M. Calvo-Dahlborg [a, b, *], U. Dahlborg [a, b], J. Cornide [a, 1], S. Mehraban [b], Z. Leong [c], T.C. Hansen [d], R.K. Wunderlich [e, 2], R. Goodall [c], N.P. Lavery [b], S.G.R. Brown [b]

[a] GPM, CNRS-UMR6634, University of Rouen Normandie, Campus Madrillet, BP12, 76801, St-Etienne-du-Rouvray, France
[b] College of Engineering, Swansea University, Bay Campus, Fabian Way, Skewen, Swansea, SA1 8EN, UK
[c] Department of Materials Science and Engineering, Sheffield University, Sir Robert Hadfield Building, Mappin Street, Sheffield, S1 3JD, UK
[d] Institut Laue Langevin, 71 Avenue des Martyrs, 38042, Grenoble Cedex 9, France
[e] Institut für funktionelle Nanosysteme, Universität Ulm, Albert-Einstein-Allee 47, D-89081, Ulm, Germany

ARTICLE INFO

*Article history:*
Received 18 March 2020
Received in revised form
2 May 2020
Accepted 4 May 2020
Available online 11 May 2020

*Keywords:*
High entropy alloys
Multicomponent
Structure
Phases
Calorimetry
e/a

ABSTRACT

High Entropy Alloys (HEA) can be classified in three domains according to their e/a and r values, with e/a, the number of itinerant valence electrons and r the average radius for a 12 nearest atoms neighborhood. The phase composition, thermal stability and possible phase transformations of a series of HEA alloys, $CoCr_zFeNi$-XY (with X and Y = Al, Cu, Pd, Ru, Ti and z = 0 or 1), selected according to their e/a ratio were investigated in cast conditions (T0), after 3 h homogenization at 1100 °C (T1) and after 3 h annealing at 700 °C (T3). When observing the behavior of the different Domains of HEAs as classified by electronic structure it is observed that for the alloys from Domain I which contain fcc structures, the microstructure transforms from multi-to almost single-phase under homogenization (T1). In Domain III alloys containing cubic (bcc and/or B2) structures, very small multi-structural changes are observed. Alloys in Domain II have a mixed structure, i.e. several different structures in the diffraction pattern, which changes during heat treatments.



## 1. Introduction

The term "high entropy alloys" (HEA) was introduced in 2004 to designate alloys consisting of 5 or more principal elements in equi- or near-equimolar amounts (5–35 at%), being single-phased and having simple crystalline structures [1]. The notion of high entropy refers to their high entropy of mixing. During the 15 years these alloys have been intensely investigated with respect to phase composition, microstructure, as well as thermal, magnetic and mechanical properties. However, in the course of these investigations it was shown that due to a unique combination of crystalline structures and microstructures several HEAs can potentially outcompete conventional alloys today in use in specific technological applications [2–5]. Thus, a new approach to metallurgy has emerged in that all elements have to be considered on an equal footing during the solidification process. This is different as compared to traditional technical alloys which usually consist of a leading ternary or binary system, such as for example Ti–Al, while the other elements can be considered as minor additions. Thus, the designation, "multi-principal element alloys", is also used to define this kind of alloy [1,6].

It is now well established that HEAs can be single-structured but are not, or are almost never, single-phased [10]. The identified structures belong in most cases to the cubic close-packed (fcc-type), the body centered cubic (bcc-type) and also hexagonal close packed (hcp-type) families of structures. It should be noted,

* Corresponding author. GPM, CNRS-UMR6634, University of Rouen Normandie, Campus Madrillet, BP12, 76801, St-Etienne-du-Rouvray, France.
*E-mail addresses:* monique.calvo-dahlborg@univ-rouen.fr (M. Calvo-Dahlborg), ulf.dahlborg@univ-rouen.fr (U. Dahlborg), s.mehraban@swansea.ac.uk (S. Mehraban), zhaoyuan@sheffield.ac.uk (Z. Leong), hansen@ill.fr (T.C. Hansen), rainer.wunderlich@uni-ulm.de (R.K. Wunderlich), r.goodall@sheffield.ac.uk (R. Goodall), n.p.lavery@swansea.ac.uk (N.P. Lavery), s.g.r.brown@swansea.ac.uk (S.G.R. Brown).
[1] Now at Department of Materials Science and Engineering, IAAB, Universidad Carlos III de Madrid. Avda. Universidad 30, 28911 Leganés, Spain.
[2] Now at Metallurgy Europe, gGmbH, Magirus-Deutz-Straße 12, 89077 Ulm, Germany.

https://doi.org/10.1016/j.jallcom.2020.155496
0925-8388/

though, that the identification of crystalline structures present in a many-phase alloy is a very complicated matter and its success depends on the resolution of the experimental technique used. Since their discovery the determination of the phase stability of HEAs after solidification has been a significant issue in many investigations. Phase changes due to external fields (temperature, pressure, etc) have been found to have a profound influence on the microstructure and, thus, the mechanical and magnetic properties. The design of alloys that contain phases with specific crystalline structures is accordingly of utmost importance in order to predict physical properties. For this purpose, a combination of parameters relevant in this context have been considered for their synthesis, including aspects of phase formation, microstructure and phase stability, strengthening mechanisms, and high temperature properties, as well as the density and cost [2–5,7–9].

Recently a classification of HEAs was proposed using the average value of the electron concentration or number of itinerant electrons per atom (e/a) in the alloy and the average atomic radius calculated for a 12-atoms neighborhood [11,12]. The importance of the number of itinerant electrons per atom in understanding and predicting the phases in solid solutions was stressed as early as 1966 [13]. In Ref. [14] the use of e/a is discussed by Massalski for the determination of Hume-Rothery phases as opposed to an approach using the total number of valence electrons per atom (VEC) (which includes the d electrons). By applying this approach for HEAs as solid solutions a classification and design methodology was proposed. From the variation of the average magnetic moment per atom and the hardness as a function of e/a and the 12 atoms radius, three Domains were identified in Refs. [11,12]: Domain I containing alloys with phases with close-packed cubic structures (below denoted fcc), Domain II contains alloys with phases of a mixed and complex structural type and Domain III containing alloys with body-centered cubic structures (below denoted bcc). The atomic radii are taken from Teatum [15] as these probably are the most useful when discussing metallic alloys. They are reported for a coordination number 12 atomic structure and were obtained from observed atomic distances in face-centered cubic and hexagonal close-packed structures. The first property used for classification of HEAs was the magnetization at saturation [11,12].

The potential success of using high entropy alloys in technological applications depends on their stability following different thermal exposures. The present work focusses on the influence of heat treatments on the stability of alloys and aims to investigate common effects in the three different Domains after heat treatments. The alloys chosen for this investigation cover all Domains according to the classification above [11,12]. All contain Co, Fe and Ni as base components (abbreviated to CFN below). When Cr is also present the abbreviation CCFN is used.

## 2. Material and methods

All alloys were prepared by arc melting of pure elements, with purities higher than 99.9 wt%, under a Ti-gettered high-purity argon atmosphere [10]. The alloys were re-melted several times in order to obtain homogeneity and to minimize oxide impurities. Cylindrical rods with diameter of 3 mm were then prepared by copper-mold suction casting into a water-cooled Cu hearth. Table 1 gives the acronyms and the nominal compositions of the investigated alloys.

The crystalline structure of all samples was investigated by neutron diffraction (ND) on the D20 diffractometer at Institute Laue-Langevin (ILL), Grenoble (France). The wavelength of the incident neutrons was 1.12 Å [16]. The crystalline structure of the phases present in the alloys were determined by a refinement procedure using the DICVOL computer code [17]. The values of the lattice constants will be presented in a separate paper. As neutrons are weakly interacting with matter the refinement gives a result valid for the entire irradiated volume.

**Table 1**
Acronyms and nominal compositions of the investigated alloys.

| Acronym | Alloy nominal composition (at.%) |
|---|---|
| CCFNPd | $Co_{20}Cr_{20}Fe_{20}Ni_{20}Pd_{20}$ |
| CCFNRu | $Co_{20}Cr_{20}Fe_{20}Ni_{20}Ru_{20}$ |
| CCFNCu | $Co_{20}Cr_{20}Fe_{20}Ni_{20}Cu_{20}$ |
| CFNCu | $Co_{25}Fe_{25}Ni_{25}Cu_{25}$ |
| CCFNAl | $Co_{20}Cr_{20}Fe_{20}Ni_{20}Al_{20}$ |
| CCFNAlCu | $Co_{16.6}Cr_{16.6}Fe_{16.6}Ni_{16.6}Al_{16.6}Cu_{16.6}$ |
| CFNTi | $Co_{25}Fe_{25}Ni_{25}Ti_{25}$ |
| CCFNAlTi | $Co_{16.6}Cr_{16.6}Fe_{16.6}Ni_{16.6}Al_{16.6}Ti_{16.6}$ |
| CFNAl | $Co_{25}Fe_{25}Ni_{25}Al_{25}$ |
| CFNAlTi | $Co_{20}Fe_{20}Ni_{20}Al_{20}Ti_{20}$ |
| $CCFNAl_{1.2}$ | $Co_{19.2}Cr_{19.2}Fe_{19.2}Ni_{19.2}Al_{23.1}$ |
| $CF_{0.8}NAl_{1.2}$ | $Co_{25}Fe_{20}Ni_{25}Al_{30}$ |

In order to investigate their thermal stability, the as-cast alloys were subjected to different heat treatments. In the DSC patterns performed on most investigated samples, transitions appear around 600 and 1000 °C. Consequently, samples cut from the same ingots were annealed for 3 h at 1100 °C (T1), 700 °C (T3) or 400 °C (T2). In the following the temperature at which the samples had been heat treated will be referred to as T1, T2 and T3, and the as-cast condition as T0. The time needed to reach the required temperature was a few minutes. The heat-treated alloys were ice-water quenched in order to retain the structure. All subsequent measurements were performed at ambient temperature. 18.

Microstructures of most of the alloys presented in the manuscript have been published in other papers by the authors: CoCrFeNi, CoCrFeNiPd, CoCrFeNiRu and CoCrFeNiSn in Ref. [18]. $CoCr_xFeNiAl_y$ in Ref. [19] and $CoCrFeNiPd_x$ in Refs. [20].

The phase transformations occurring during heating to different temperatures and during the subsequent cooling were studied for selected alloys by Differential Scanning Calorimetry (DSC) with a Netzsch STA 449C instrument under a flowing nitrogen protective atmosphere. Experiments on some of the alloys were repeated several times. The rate of temperature change was in all measurements 40 $Kmin^{-1}$. It will be called “slow” in the following as opposed to “quench” for the water quench.

## 3. Results

### 3.1. Determination of the crystallographic structure of as-cast and annealed alloys by neutron diffraction

The structure of 12 selected alloys, 4 in each of the three Domains will be discussed in this work. All were investigated in the as-cast condition as well as after three different heat treatments, T1, T2 and T3, followed by water quenching. The measured diffraction patterns are presented in Figs. 1–3. For clarity the three curves for the different heat treatments have been shifted vertically and presented in the following order, from bottom to top: as-cast alloys (T0), after annealing for 3 h at 1100 °C (T1) and after annealing for 3 h at 700 °C (T3). When comparing the diffraction patterns, it is important to note that in the experiments the samples, all being ingots of different shapes and sizes, have been held in arbitrary orientations. Thus, the measured diffraction peak intensities are also affected by texture and they will therefore not necessarily give a representative estimation of the amount of a certain phase present. It should also be noted that all alloys have been produced and treated in the same way. Thus, no significant influence on the alloy phase composition due to a variation of elemental purities or of

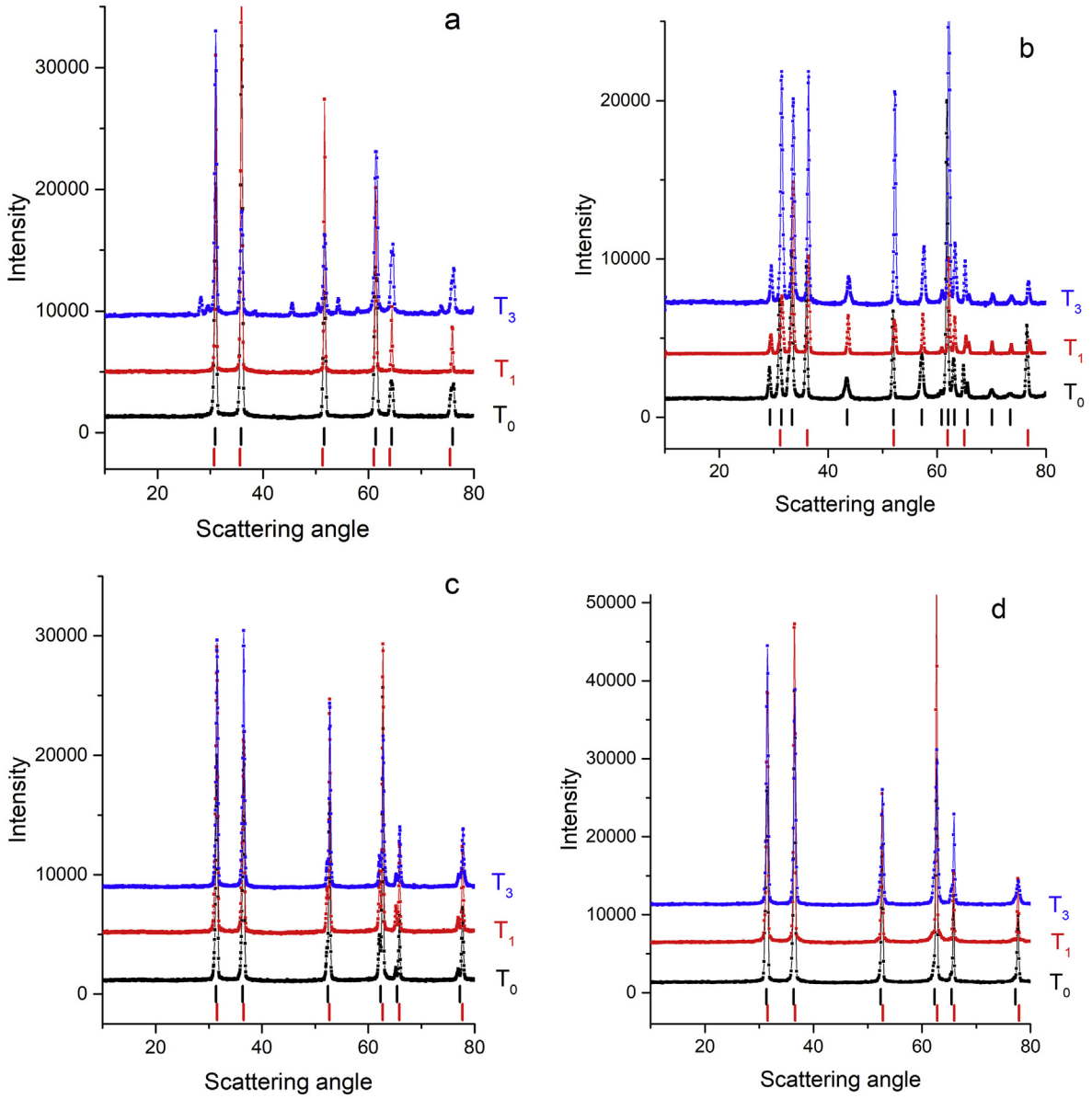


**Fig. 1.** ND patterns of the Domain I alloys: in black the as-cast (T0) condition; in red after heat treatment according to T1; and in blue after heat treatment according to T3. The alloy compositions are a) CoCrFeNiPd, b) CoCrFeNiRu, c) CoCrFeNiCu, and d) CoFeNiCu. The vertical bars correspond to diffraction peak positions of the two crystalline structures present in largest amounts in every alloy. (For interpretation of the references to colour in this figure legend, the reader is referred to the Web version of this article.)

differences in cooling rates on diffraction peak intensities is expected.

The structures identified from the diffraction patterns displayed in Figs. 1–3 are listed in Table 2. A rough relative estimate of the amount of a particular structure in columns T0, T1 and T3 is given in decreasing order going from left to right in columns T0, T1 and T3. The structure to the left belongs to the main phase. The elemental composition of the different phases/structures has not been possible to determine with sufficient accuracy even by refinement procedures and thus only the type of crystalline structure is given. The first column in Table 2 indicates the Domain to which the alloy belongs according to the classification mentioned above [11,12]. It can be seen that several alloys exhibit two phases having the same type of structure, for examples two simple fcc and one bcc in combination with a B2 structure. The assignments of phases for some alloys differ furthermore from other published works due the insufficient experimental resolution used in these publications. The derived lattice constants of the different structures are presented in our earlier works [10,21,22]. It can be noticed in Figs. 1–3 that in some patterns small peaks, indicated by question marks in Table 2, which possibly corresponds to a minority phase can be seen. As their intensities are very small and due the fact that they are very few in one pattern it has not been possible to determine the corresponding crystalline structure. However, their presence does not influence the general conclusions of the paper.

All alloys of a specific Domain were found to have the type of structure in the as-cast state that would be predicted by the classification scheme described above [12]. Thus, in Domain I alloys with fcc or hcp structures are found while the alloys in domain III contain structures of bcc type. The alloys in domain II consist of a mixture of fcc and bcc structure types. The $L2_1$ structure is observed for a few alloy compositions and also after

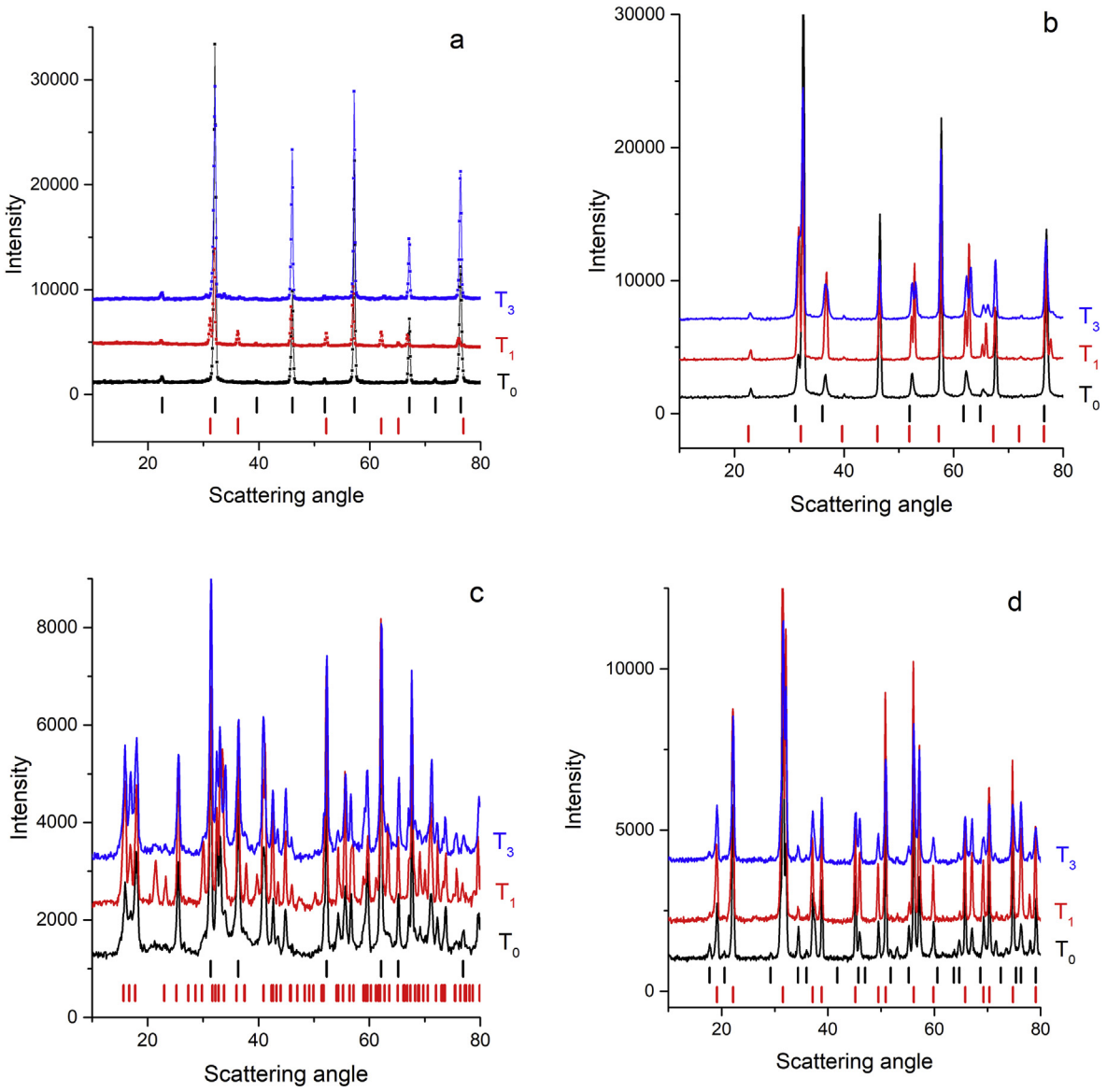


**Fig. 2.** ND patterns of the Domain III alloys: in black the as-cast (T0) condition; in red after heat treatment according to T1; and in blue after heat treatment according to T3. The alloy compositions are a) CoFeNiAl, b) CoFeNiAlTi, c) $CoCrFeNiAl_{1.2}$, and d) $CoFe_{0.8}NiAl_{1.2}$. The vertical bars correspond to diffraction peak positions of the two crystalline structures present in largest amounts in every alloy. (For interpretation of the references to colour in this figure legend, the reader is referred to the Web version of this article.)

different heat treatments. It is a complex structure and contains atoms in both octahedral and tetrahedral interstitial positions with all atoms located on the sites of a body-centered cubic lattice.

On heat treatment the alloys of a particular Domain behave similarly. The investigated alloys of Domain I retain fcc and hcp phases after both T1 and T3 heat treatments (see Fig.1 a to d). Alloys of Domain III retain phases of bcc types (see Fig 2 a to d) and alloys of Domain II retain their mixed phase composition (see Fig. 3 a to d). Another result from Table 2 is that removing Cr from one alloy sometimes drives the alloy from one Domain to another (e.g. CCFNAlTi and CCFNAl in Domain II, CFNAlTi and CFNAl in Domain III) and sometimes not (e.g. CCFNCu and CFNCu in Domain I). It is also interesting to note that a small change in the relative Al amount of an alloy can have the same effect (e.g. CCFNAl in Domain II and $CCFNAl_{1.2}$ in Domain III). Both these effects depend on compared values of e/a and r [12].

### 3.2. Calorimetric studies

In order to obtain further information on the thermal stability of the alloy structures differential scanning calorimetry (DSC) measurements were performed on one alloy from each Domain: CCFNPd from Domain I, CCFNAl from Domain II and CFNAl from Domain III. The heating/cooling rate was 40 $Kmin^{-1}$ for all measurements, which were all performed under continuous nitrogen gas flow. It should be noted that all studied alloys have melting points above 1400 °C and that the solidification took place during slow cooling (as compared for rapid cooling used e.g. for the formation of metallic glasses). The alloys were investigated according to different heat treatment schemes:

- A. Heating from room temperature (RT) to 1500 °C on an as-cast sample previously annealed to T1 (3 h at 1100 °C and subsequently water-quenched).

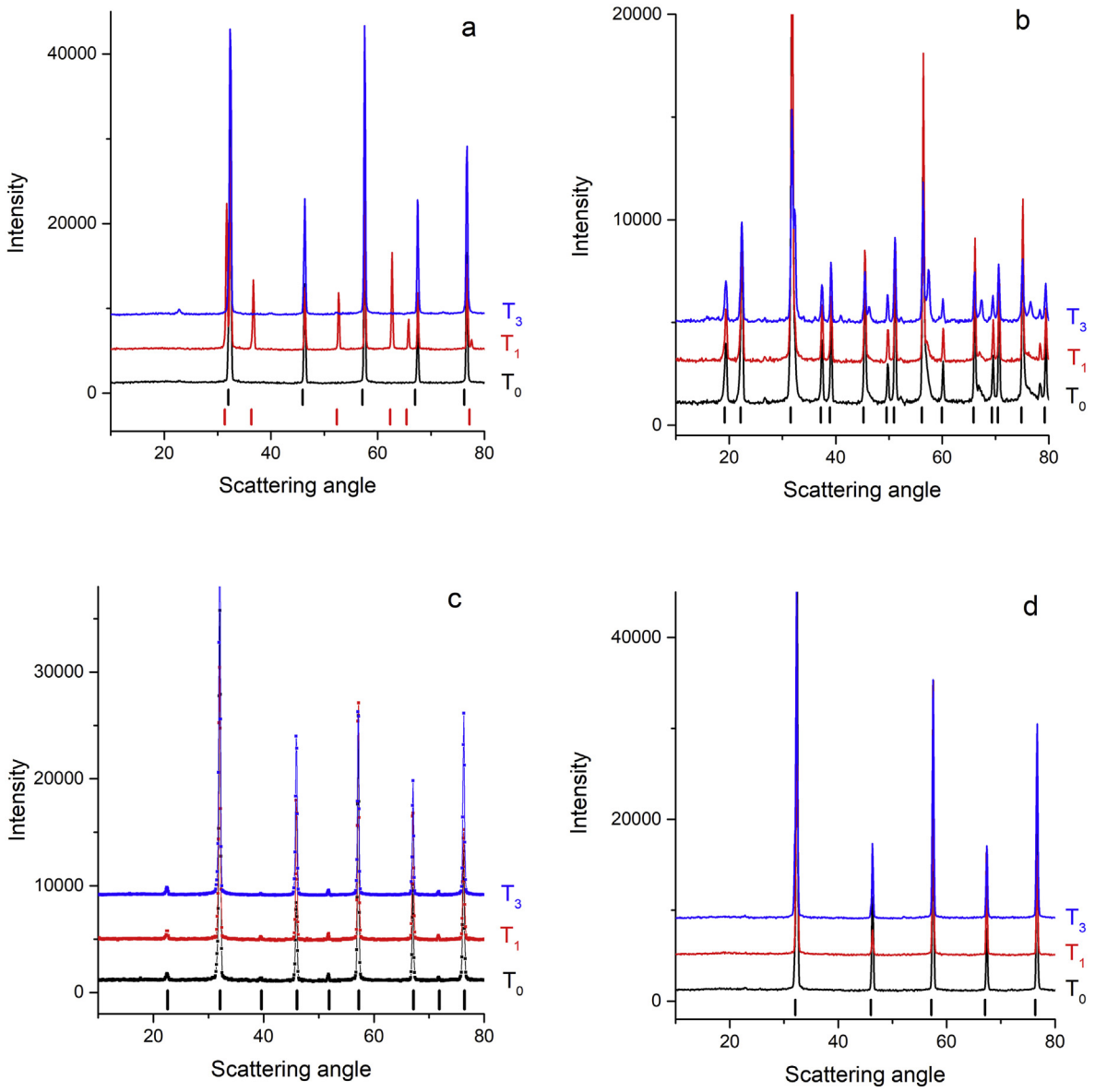


**Fig. 3.** ND patterns of the Domain II alloys: in black the as-cast (T0) condition; in red after heat treatment according to T1; and in blue after heat treatment according to T3. The alloy compositions are a) CoCrFeNiAl, b) CoCrFeNiAlCu, c) CoFeNiTi and d) CoCrFeNiAlTi. The vertical bars correspond to diffraction peak positions of the two crystalline structures present in largest amounts in every alloy. (For interpretation of the references to colour in this figure legend, the reader is referred to the Web version of this article.)

**Table 2**
List of the crystalline structures observed in alloys in as-cast condition (T0) as well as after heat treatments T1 and T3 defined in the text. The specified structures are the simple face-centered cubic (fcc), the simple body-centered cubic (bcc), the ordered body-centered cubic (B2), the Heusler ($L2_1$), and the hexagonal close-packed (hcp) structural type. The presence of unidentified structure is denoted by (?). The first column indicates the domain to which the alloy belongs according to the classification discussed in Refs. [11,12].

| Domain | Alloy | As-cast (T0) | | | | After annealing (T1) | | | | After annealing (T3) | | | |
|---|---|---|---|---|---|---|---|---|---|---|---|---|---|
| I | CCFNPd | fcc | fcc | | | fcc | | | | fcc | fcc | ? | |
| | CCFNRu | hcp | fcc | | | hcp | fcc | | | hcp | fcc | | |
| | CCFNCu | fcc | fcc | | | fcc | fcc | | | fcc | fcc | | |
| | CFNCu | fcc | fcc | | | fcc | fcc | | | fcc | fcc | | |
| II | CCFNAl | bcc | fcc | B2 | | bcc | fcc | B2 | | bcc | B2 | ? | |
| | CCFNAlCu | bcc | fcc | B2 | | bcc | fcc | fcc | B2 | bcc | fcc | fcc | B2 |
| | CFNTi | hcp | fcc | ? | | hcp | fcc | ? | | hcp | fcc | ? | |
| | CCFNAlTi | $L2_1$ | $L2_1$ | fcc | bcc | $L2_1$ | bcc | ? | | $L2_1$ | $L2_1$ | fcc | bcc |
| III | CFNAl | bcc | B2 | | | bcc | fcc | | | bcc | B2 | | |
| | CFNAlTi | $L2_1$ | ? | | | $L2_1$ | ? | | | $L2_1$ | ? | | |
| | $CCFNAl_{1.2}$ | bcc | B2 | | | bcc | B2 | | | bcc | B2 | | |
| | $CF_{0.8}NAl_{1.2}$ | bcc | | | | bcc | | | | bcc | B2 | | |

- B. Heating from RT to 1500 °C of an as-cast sample previously annealed to T3 (3 h at 700 °C and subsequently water-quenched).
- $C_i$ (i = 1,3). Heating/cooling of an as-cast sample according to the temperature variational scheme shown in Fig. 4. That is:
  - $C_1$: Heating of an as-cast sample from RT to 1100 °C and subsequently cooled at the same rate (40 K/min).
  - $C_2$: Heating of sample $C_1$ from RT to 700 °C and subsequently cooled at the same rate (40 K/min).
  - $C_3$: Heating of sample $C_2$ from RT to 1500 °C and subsequently cooled at the same rate (40 K/min).

The heat flow curves for Domains I, III and II, measured during heating, are shown in Figs. 5a, 6a and 7a while the differentiated counterparts are displayed in Figs. 5b, 6b and 7b, respectively. The differentiated curves help in detecting occurrences of specific features and may expose differences between different alloys more clearly. Several phase transformations obviously occur in all alloys during the different heating schemes. The main structural events are identified as those that take place by a temperature change in the observed curves of more than ~0.2 °C over a time period of 10 s. Some small variations in heat flow are nevertheless considered to be real if they are observed in several DSC heat flow curves.

## 4. Discussion

When comparing and interpreting the diffraction measurements in combination with the DSC studies it should be noted that the alloys were not investigated under completely comparable circumstances by the two techniques. For experimental reasons the maximum temperature achievable in the neutron diffraction measurements was too low in order to duplicate the DSC measurements. Thus, all diffraction measurements were performed at ambient temperature on both the as-cast and on the heat-treated alloys, whereas the DSC measurements were performed with a constant heating rate. Consequently, some features seen in the DSC curves may not be detected in the diffraction experiments and vice versa as the response to structural phase changes is different. In particular, because of the sluggish diffusion predicted/observed for many HEA alloys, DSC heat flow features and, thus, the underlying material transformations, may be dependent on heating and cooling rates.

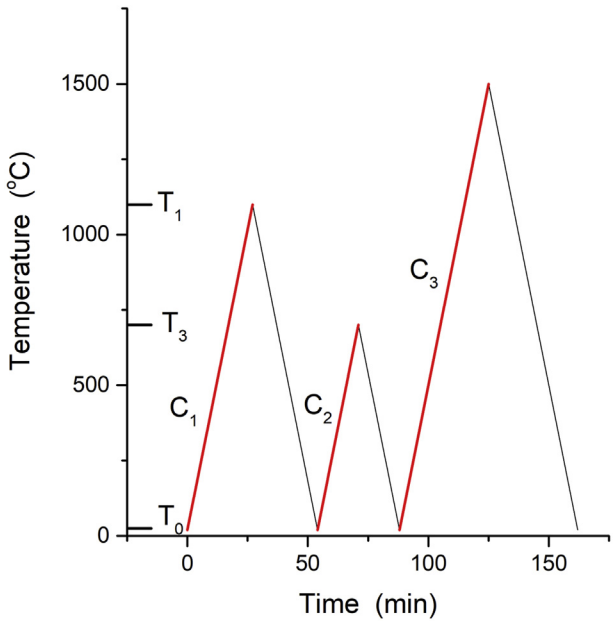


**Fig. 4.** Temperature variational scheme applied during DSC measurements of as-cast alloys previously heated to 1100 °C and subsequently cooled with a rate of 40 K/min.

### 4.1. Domain I alloys

The diffraction patterns shown in Fig. 1 and the reported structures identified in Table 2 show that the two annealing procedures T1 and T3 do not change the overall crystalline structures of the alloys as compared to the as-cast phase composition. Only two different structures are observed, namely fcc and hcp. The corresponding diffraction peak positions are shown as vertical bars in Fig. 1. The only exception is the CCFNPd alloy for which the diffraction pattern exhibits several additional peaks after the T3 heat treatment implying the presence of a third structure. It was suggested in Refs. [10] that these originated from a slightly distorted fcc structure (actually a monoclinic structure with a very similar lattice constant). This view is supported by the DSC results discussed below.

The features observed in the DSC heat flow curves (Fig. 5a and b) at temperatures less than 1200 °C for CCFNPd alloy are summarized in Table 3. In order to substantiate the magnitude, small features are listed within parentheses and the trace ones within double parentheses. The melting temperature is found to be nearly the same in all the heating schemes and is found in the range 1276 ± 4 °C. The identified features are represented by vertical bars in Fig. 5a.

The as-cast CCFNPd alloy exhibits many structural transformations when heated to 1100 °C (scheme $C_1$). Some of these are reversible and can be seen again during the second heating after heat treatments T1 and T3. The phase transformation occurring at the temperature $T_a$ clearly takes place irrespective of the previous heat treatments. It is very distinct after T1 and T3 but it is rather faint in the $C_3$ heating. The corresponding phase has obviously grown during the 3 h annealing time which shows the influence of both cooling rate and annealing time on the alloy phase composition. The DSC curves measured in the C sequence are very similar and show that the T1 and the T3 treatments when followed by slow cooling (40 K/min) do not affect the alloy phase content significantly. Thus, all structural changes are reversible in this case. Moreover, the thermal signal at Ta does not resemble that of a first order phase transition but a slow dissolution of some phase or a thermally activated precipitation reaction. However, the reversibility excludes a precipitation reaction but reminds of a binary eutectic phase diagram when a hypereutectic composition is heated.

The diffraction measurements indicate that a new phase was formed in the CCFNPd alloy after the T3 treatment (Fig. 1a). It might be conjectured that this corresponds to the transformation taking place at the temperature $T_c$. As the transformation probably is of diffusive nature it has been initiated but not completed during the 3 h the alloy was kept at 700 °C. This finding corroborates the observation of a generally sluggish kinetics in HEA alloys.

It can be concluded that the crystalline structure of Domain I alloys does not change during heat treatments at the selected temperatures, except at T3. All identified phases in this Domain are of fcc and/or hcp type (Table 2). Structural changes, both reversible and irreversible, might occur due to different heat treatments but all phases remain of this type.

### 4.2. Domain III alloys

Some diffraction patterns of alloys that have been classified in Ref. [11,12] to belong to Domain III are shown in Fig. 2. Only diffraction peak positions corresponding to the two major

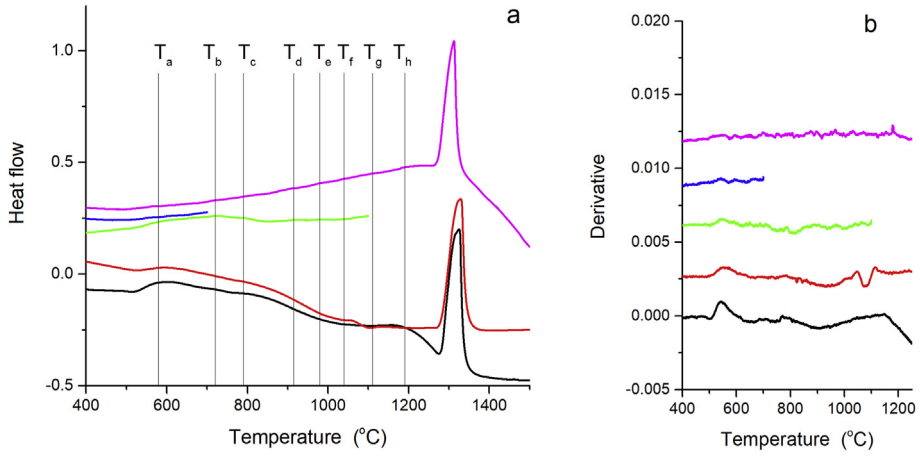


**Fig. 5.** Domain I, CCFNPd: (a) DSC heat flow curves and (b) their derivative. The curves are shifted vertically in the following order from bottom: Scheme A (black), scheme B (red), scheme $C_1$ (green), scheme $C_2$ (blue), scheme $C_3$ (magenta). The vertical lines correspond approximately to the temperature in the corresponding column in Table 3. (For interpretation of the references to colour in this figure legend, the reader is referred to the Web version of this article.)

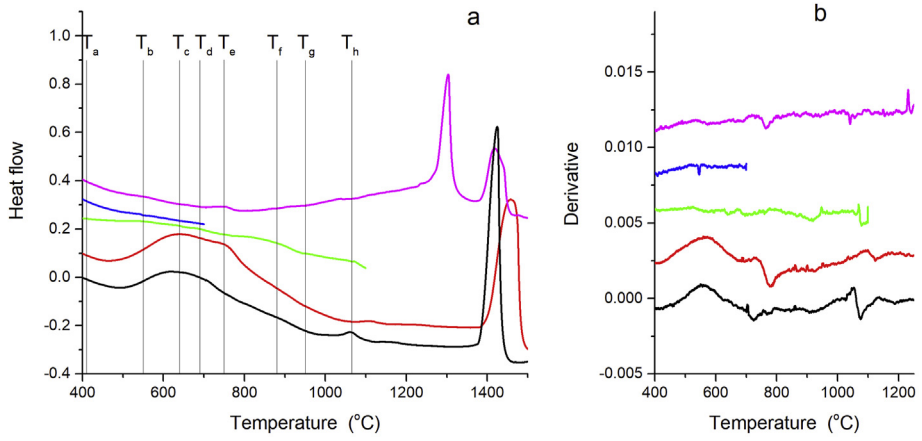


**Fig. 6.** Domain III, CFNAl: (a) DSC heat flow curves and (b) their derivative. The curves are shifted vertically in the following order from bottom: Scheme A (black), scheme B (red), scheme $C_1$ (green), scheme $C_2$ (blue), scheme $C_3$ (magenta). The vertical lines correspond approximately to the temperature in the corresponding column in Table 4. (For interpretation of the references to colour in this figure legend, the reader is referred to the Web version of this article.)

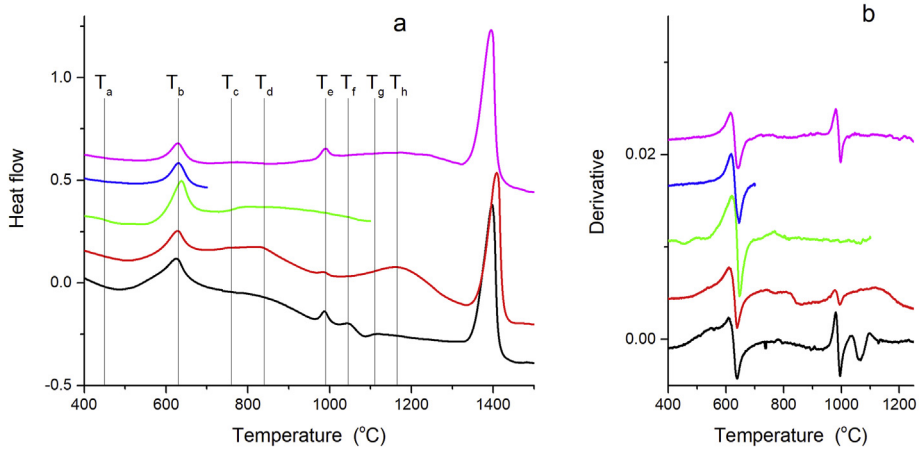


**Fig. 7.** Domain II, CCFNAl: (a) DSC heat flow curves and (b) their derivative. The curves are shifted vertically in the following order from bottom: Scheme A (black), scheme B (red), scheme $C_1$ (green), scheme $C_2$ (blue), scheme $C_3$ (magenta). The vertical lines correspond approximately to the temperature in the corresponding column in Table 5. (For interpretation of the references to colour in this figure legend, the reader is referred to the Web version of this article.)

**Table 3**
Domain I, CCFNPd: Temperatures in °C of thermal features identified in the DSC heat flow curves of CCFNPd in the different heating schemes (see above). In order to substantiate the magnitude, small features are listed within parentheses and the trace ones within double parentheses.

| Measurement | $T_a$ | $T_b$ | $T_c$ | $T_d$ | $T_e$ | $T_f$ | $T_g$ | $T_h$ |
|---|---|---|---|---|---|---|---|---|
| A | 580 | (717) | 793 | | | (1036) | | |
| B | 587 | | ((793)) | | (991) | 1057 | 1110 | |
| $C_1$ | 593 | (727) | 791 | 916 | 987 | (1041) | | |
| $C_2$ | (561) | | | | | | | |
| $C_3$ | (590) | (720) | (797) | 917 | 980 | (1040) | | 1190 |

structures are displayed as vertical bars. Structures present are mainly bcc, $L2_1$ and B2 in as-cast state with appearance of fcc after T1 treatment in some alloys, e.g. CFNAl. It is noticed that the structural content of an alloy is very sensitive to composition. For example, comparing Fig. 2a and d it is seen that a small change in the Fe and Al content results in a disappearance of the fcc structure from the CFNAl alloy after the T1 treatment. Removing Cr from the CCFNAl alloy (Fig. 2c) causes the disappearance of the B2 structure (Fig. 2d).

The CFNAl was also investigated by DSC measurements according to the temperature variation schemes mentioned above. The features observed in the DSC heat flow curves shown in Fig. 6 are summarized in Table 4. The identified features are represented by vertical bars. The general shapes of the curves are very different from the ones measured for the CCFNAl alloy (see Fig. 7) indicating that the temperature behavior is sensitive to the Cr content. A very striking observation is that the melting takes place in two stages after scheme $C_3$. The sum of areas of the two peaks is close to the areas of the corresponding peaks measured after schemes A and B. This suggests that the alloy consists of two phases after schemes $C_1$ and $C_2$. The temperatures at which the melting processes take place $T_{m1}$ and $T_{m2}$ are shown in Table 4.

Comparison of the heat flow curves of the 3 h T1 and T3 annealed CFNAl specimen, curves A and B, with that of the as-cast specimen exposed to the heating schemes $C_1$, $C_2$ and $C_3$ in sequence show a significant difference. Curves A and B exhibit a distinct broad endothermal event starting at $T = 520 \pm 20$ °C which is absent in the $C_1$, $C_2$ and $C_3$ heat flow curves. Moreover, the endothermal signal is more pronounced, i. e. the relative heat flow change is larger, for the Domain III than for the Domain I alloy. This implies that during annealing for 3 h at 700 °C and 3 h at 1100 °C a new or additional phase was formed which was retained on the subsequent water quenching. Obviously, this phase was not formed in the $C_1$–$C_2$–$C_3$ heating scheme. As the corresponding heat flow curves give no indication of a corresponding exothermal signal it cannot be argued that such a phase was formed on heating but did dissolve in the 40 K/min cooling. As such, it can be concluded that the formation of this phase is very much dominated by slow kinetics during annealing. Comparing the A and B curves shows that in curve B, corresponding to the heat flow signal of the 3 h at 700 °C annealed specimen, the endothermal signal starting at $T = 520$ °C is larger than that in curve A, indicating that the amount of that phase is larger for the 700 °C than for the 1100 °C annealing. Accordingly, these observations indicate that this alloy exhibits phase transformation on annealing at intermediate temperatures and that the room temperature phase composition may critically depend on the thermal history of the alloy.

The transformation with onset at Tb may correspond to the transformation at Tb at about 630 °C that was observed for the Domain II CCFNAl alloy (see Table 5). Some features disappear when the annealing is followed by a slow cooling ($C_3$).

It can be concluded that the crystalline structure type of alloys classified to belong to Domain III does not change during heat treatments. All identified crystalline structures in this domain are of bcc, B2 or L21 type (Table 2). The alloy phase content depends on the rate of temperature changes. The T1 and T3 heat treatments followed by quench (A and B) seem to stabilize some of the phases. Some features disappear when the annealing is followed by a slow cooling ($C_3$). The slow cooling stabilizes only the $T_d$ transformation.

### 4.3. Domain II alloys

ND diffraction patterns of the selected Domain II alloys exposed to different heat treatments, T0, T1 and T3 are shown in Fig. 3 a – d. All contain structures of fcc and bcc type irrespective of heat treatments. Only diffraction peak positions corresponding to the two major structures are displayed as vertical bars. Thus, the clearly visible peaks that correspond to the B2 structure in Fig. 2a and b are not explicitly shown. There does not seem to be a uniform behavior of the alloys in this domain on any of the heat treatments T1 and T3 in that for some new structures appear and for some not.

From this domain the CCFNAl alloy was selected for DSC measurements according to the temperature schemes mentioned above. The DSC heat flow curves are shown in Fig. 7. The temperatures at which distinct thermal features are observed are listed in Table 5. The identified features are indicated by vertical bars in Fig. 7. The onset of melting for schemes A and $C_3$ was found as $T_{ons} = 1350$°**C** while after scheme B it was somewhat higher, at 1363 °C.

From the shape of the DSC curves it can be concluded that the phase composition of this alloy is affected more significantly by temperature changes than the CCFNPd alloy belonging to Domain I. Two main transformations occur, one reversible at about 630 °C ($T_b$ in Table 5) and one partly reversible at about 990 °C ($T_e$ in Table 5). The fcc structure observed in the diffraction pattern of this alloy

**Table 5**
Temperature in °C of distinct thermal features in the DSC heat flow curves recorded for CCFNAl. In order to substantiate the magnitude, small features are listed within parentheses and the trace ones within double parentheses.

| Measurement | $T_a$ | $T_b$ | $T_c$ | $T_d$ | $T_e$ | $T_f$ | $T_g$ | $T_h$ |
|---|---|---|---|---|---|---|---|---|
| A | | 627 | 776 | | 988 | 1048 | 1110 | |
| B | ((506)) | 629 | 757 | 831 | 988 | ((1071)) | | 1165 |
| $C_1$ | (443) | 638 | 754 | (850) | (991) | (1056) | | |
| $C_2$ | ((527)) | 630 | | | | | | |
| $C_3$ | | 629 | (764) | (858) | 990 | ((1056)) | | |

**Table 4**
Domain III, CFNAl: Temperatures in °C of thermal features identified in the DSC heat flow curves of CFNAl in the different heating schemes (see above). In order to substantiate the magnitude, small features are listed within parentheses and the trace ones within double parentheses.

| Measurement | $T_a$ | $T_b$ | $T_c$ | $T_d$ | $T_e$ | $T_f$ | $T_g$ | $T_h$ | $T_{m1}$ | $T_{m2}$ |
|---|---|---|---|---|---|---|---|---|---|---|
| A | | | 630 | 707 | | (890) | | 1064 | | 1384 |
| B | | | 644 | | 752 | | | 1106 | | 1400 |
| $C_1$ | (405) | (548) | (633) | (684) | | (873) | 948 | (1072) | | |
| $C_2$ | | 545 | | | | | | | | |
| $C_3$ | ((475)) | (559) | | | 753 | | | (1040) | 1274 | 1389 |

after the T1 annealing and not after the T3 can thus be correlated with the $T_e$ feature in the DSC curve.

It can be concluded that the crystalline structure of Domain II alloys significantly undergoes considerable changes during heat treatments. This is obvious due to the presence in these alloys of mixed phases, e.g. metastable phases, intermetallics, sigma, etc. These phases naturally grow or transform to more stable phases under heat treatments. Thus, structural changes, both reversible and irreversible, might occur due to different heat treatments.

## 5. Conclusion

1) All alloys belonging to a specific Domain have been found to have the type of structure in the as-cast state as predicted by the classification scheme given in Refs [11,12]. Thus, in Domain I alloys with fcc or hcp structures are found while the alloys in Domain III contain structures of bcc type. The alloys in Domain II form both fcc and bcc structures as well as other intermetallics.
2) Removing Cr from one alloy can drive the alloy from one Domain to another. A small change in the relative Al amount of an alloy can have the same effect. Both effects depend on the resulting values of e/a and r [12].
3) The investigated alloys of Domain I exhibit only one type of structure independent of heat treatment. The microstructure transforms from multi-to almost single-phase under homogenization at T = 1100 °C. Annealing at 700 °C leads to additional phases depending on the cooling procedure after annealing.
4) Alloys of Domain II undergo more phase transformations during the different heat treatments than the investigated Domain I alloy. The alloys contain both fcc and bcc phases (being of mixed type) and are still of mixed type after heat treatment. Most of the phases present in as-cast samples remain after heat treatment at 1100 and 700 °C indicating a pronounced structural instability of the alloy with regard to temperature variations.
5) Alloys from Domain III present more transformations in the as cast sample than for Domain I and II alloys but these features are much smaller. The 1100 and 700 °C heat treatments followed by quench seem to stabilize some of the phases. The alloy phase composition is very sensitive to the rate of cooling.
6) The rate of cooling after annealing at 1100 and 700 °C influences the phase composition This a very important result for the homogenization procedure often performed on HEAs, depending in which Domain their compositions locate them.

## Declaration of competing interest

The authors declare that they have no known competing financial interests or personal relationships that could have appeared to influence the work reported in this paper.

## CRediT authorship contribution statement

**M. Calvo-Dahlborg:** Conceptualization, Writing - original draft, Supervision. **U. Dahlborg:** Formal analysis, Investigation, Writing - original draft, Validation. **J. Cornide:** Formal analysis, Investigation. **S. Mehraban:** Formal analysis, Investigation. **Z. Leong:** Formal analysis, Investigation. **T.C. Hansen:** Formal analysis, Investigation. **R.K. Wunderlich:** Validation, Writing - review & editing. **R. Goodall:** Writing - review & editing. **N.P. Lavery:** Resources, Writing - review & editing. **S.G.R. Brown:** Writing - review & editing.

## Acknowledgements

The authors are thankful to Institute Laue-Langevin, Grenoble, France, for awarding beam-time on the D20 diffractometer at the ILL reactor. The present work has been carried out within the FP7 European project AccMet NMP4-LA-2011-263206. Some of the DSC measurements have been performed on installations founded by the COMET project at Swansea University.

## References

[1] J.W. Yeh, S.K. Chen, S.J. Lin, J.Y. Gan, T.S. Chin, T.T. Shun, C.H. Tsau, S.Y. Chang, Nanostructured high-entropy alloys with multiple principal elements: novel alloy design concepts and outcomes, Adv. Eng. Mater. 6 (2004) 299–303, https://doi.org/10.1002/adem.200300567.
[2] M.C. Gao, J.W. Yeh, P.K. Liaw, Y. Zhang, High-Entropy Alloys: Fundamentals and Applications, Springer, 2016.
[3] Y. Zhang, T.T. Zuo, Z. Tang, M. C Gao, K.A. Dahmen, P.K. Liaw, Z.P. Lu, Microstructures and properties of high-entropy alloys, Prog. Mater. Sci. 61 (2014) 1–93, https://doi.org/10.1016/j.pmatsci.2013.10.001.
[4] D.B. Miracle, O.N. Senkov, A critical review of high entropy alloys and related concepts, Acta Mater. 122 (2017) 448–511, https://doi.org/10.1016/j.actamat.2016.08.081.
[5] D.B. Miracle, J.D. Miller, O.N. Senkov, C. Woodward, M.D. Uchic, J. Tiley, Exploration and development of high entropy alloys for structural applications, Entropy 16 (2014) 494–525, https://doi.org/10.3390/e16010494.
[6] O.N. Senkov, J.D. Miller, D.B. Miracle, C. Woodward, Accelerated exploration of multi-principal element alloys with solid solution phases, Nat. Commun. 6 (2015) 6529, https://doi.org/10.1038/ncomms7529.
[7] X. Yang, Y. Zhang, Prediction of high-entropy stabilized solid-solution in multi-component alloys, Mater. Chem. Phys. 132 (2012) 233–238, https://doi.org/10.1016/j.matchemphys.2011.11.021.
[8] M.H. Tsai, J.W. Yeh, High-entropy alloys: a critical review, Mater. Res. Lett. 2–3 (2014) 107–123, https://doi.org/10.1080/21663831.2014.912690.
[9] Z.P. Lu, H. Wang, M.W. Chen, I. Baker, J.W. Yeh, C.T. Liu, T.G. Nieh, An assessment on the future development of high-entropy alloys: summary from a recent workshop, Intermetallics 66 (2015) 67–76, https://doi.org/10.1016/j.intermet.2015.06.021.
[10] U. Dahlborg, J. Cornide, M. Calvo-Dahlborg, T. Hansen, A. Fitch, Z. Leong, S. Chambreland, R. Goodall, Structure of some CoCrFeNi and CoCrFeNiPdx multicomponent HEA alloys by diffraction techniques, J. Alloys Compd. 681 (2016) 330–341, https://doi.org/10.1016/j.jallcom.2016.04.248.
[11] M. Calvo-Dahlborg, S.G.R. Brown, Hume-Rothery for HEA classification and self-organizing map for phases and properties prediction, J. Alloys Compd. 724 (2017) 353–364, https://doi.org/10.1016/j.jallcom.2017.07.074.
[12] M. Calvo-Dahlborg, U. Dahlborg, S.G. Brown, J. Juraszek, Influence of the electronic polymorphism of Ni on the classification and design of high entropy alloys, J. Alloys Compd. 824 (2020) 153895, https://doi.org/10.1016/j.jallcom.2020.153895.
[13] C.S. Barrett, T.B. Massalski, Structure of Metals, third ed., McGraw-Hill, 1966, pp. 306–379.
[14] T.B. Massalski, Comments concerning some features of phase diagrams and phase transformations, Mater. Trans. 51 (2010) 583–596, https://doi.org/10.2320/materia.49.192.
[15] E.T. Teatum, K.A. Gschneidner Jr., J.T. Waber, Report LA-4003. UC-25. Metals, Ceramics and Materials, Los Alamos Scientific Laboratory, 1968. TID-4500.
[16] U. Dahlborg, M. Calvo-Dahlborg, J. Cornide, R. Goodall, T. Hansen, Z. Leong, E. Suard, I. Todd, Structure of High Entropy Alloys, Institut Laue-Langevin (ILL), 2014, https://doi.org/10.5291/ILL-DATA.1-01-140.
[17] A. Boultif, D. Louër, Powder pattern indexing with the dichotomy method, J. Appl. Crystallogr. 37 (2004) 724–731, https://doi.org/10.1107/S0021889804014876.
[18] J. Cornide, U. Dahlborg, Z. Leong, L. Asensio Dominguez, J. Juraszek, S. Jouen, T. Hansen, R. Wunderlich, S. Chambreland, I. Todd, R. Goodall, M. Calvo-Dahlborg, Structure and Properties of Some CoCrFeNi-Based High Entropy Alloys, The Minerals,Metals & Materials Society, Orlando (USA), 2015, https://doi.org/10.1002/9781119093466.ch139. TMS2015.
[19] J. Cieslak, J. Tobola, J. Przewoznik, K. Berent, U. Dahlborg, J. Cornide, S. Mehraban, N. Lavery, M. Calvo-Dahlborg, Multi-phase nature of sintered vs. arc-melted CrxAlFeCoNi high entropy alloys - experimental and theoretical study, J. Alloys Compd. 801 (2019) 511–519, https://doi.org/10.1016/j.jallcom.2019.06.121.
[20] J. Cornide, M. Calvo-Dahlborg, S. Chambreland, L. Asensio Dominguez, Z. Leong, A. Cunliffe, R. Goodall, I. Todd, Combined atom probe tomography and TEM investigations of CoCrFeNi, CoCrFeNi-pdx (x=0.5, 1.0, 1.5) and CoCrFeNi-Sn, Acta Phys. Pol., A 128 (2015) 557–560, https://doi.org/10.12693/APhysPolA.128.557.
[21] M. Calvo-Dahlborg, J. Cornide, U. Dahlborg, S. Chambreland, G.D. Hatton, , et al.A. Fones, Structure and microstructural characterization of CoCrFeNiPd high

entropy alloys, Solid State Phenom. 257 (2016) 72–75. https://www.scientific.net/SSP.257.72.
[22] M. Calvo-Dahlborg, J. Cornide, J. Tobola, D. Nguyen-Manh, J.S. Wróbel, J. Juraszek, S. Jouen, U. Dahlborg, Interplay of electronic, structural and magnetic properties as driving feature of high entropy CoCrFeNiPd alloys, J. Phys. D Appl. Phys. 50 (12pp) (2017) 185002, https://doi.org/10.1088/1361-6463/aa62ea.